Mine Water and the Environment (2022) 41:790–801
https://doi.org/10.1007/s10230-022-00879-2

TECHNICAL ARTICLE

Surface Soil Water Content Before and After Coal Mining and its Influencing Factors—A Case Study of the Daliuta Coal Mine in Shaanxi Province, China

Zhiyuan Wu[1,2] · Fan Cui[2] · Junli Nie[3]

Received: 28 August 2020 / Accepted: 5 May 2022 / Published online: 18 May 2022

Abstract
The spatial variability in soil water content in the Daliuta mining area in western China was studied before and after coal mining using ground penetrating radar and geostatistical methods. The relationships among soil water content, soil physical properties, topographical factors, and vegetation density were analysed using classical statistics. The average surface soil water content changed slightly between the two detection events at the centre of the subsidence, from 0.084 cm^3/cm^3 to 0.079 cm^3/cm^3; there, the distribution of the soil water content was more closely related to terrain than any of the other factors being considered. Along the subsidence boundary, the surface soil water content decreased significantly after mining, from 0.099 cm^3/cm^3 to 0.083 cm^3/cm^3 at one location. The total soil porosity, soil organic matter, and soil clay content were positively correlated with soil water content before mining. However, after mining, the relationship between total soil porosity and soil water content significantly strengthened while the relationships between other soil physical and chemical properties and soil water content weakened. Vegetation was determined to be the main factor controlling the surface soil water content before and after coal mining at one location in a small (1,600 m^2) area of the subsidence boundary.

Keywords Geostatistics. Soil physical and chemical characteristics. Ground-penetrating radar. Vegetation density

Introduction

Underground coal mining in the Shendong mining area are necessary to ensure China's national supply of high-quality steam coal and China's national economy. However, it is a fragile eco-environmental area, featuring intense evaporation and scarce rainfall (Du 2010; Liu et al. 2017; Song 2007; Yao 2012; Zhao 2005; Zhang 2009). In addition, coal mining has disturbed the already extremely fragile eco-environment by causing subsidence and an enormous loss of water resources (Kratzseh 1986; Wei et al. 2015). Therefore, identifying the master factors controlling changes in the surface SWC distribution before and after mining is a crucial link for the environmental rectification of the mining area and its ecological recovery.

Soil water content (SWC) plays an important role in controlling vegetation growth as well as the surface ecological environment and helps prevent soil desertification (Booth et al. 2006; Huisman et al. 2001; Weihermuller et al. 2007; Wang et al. 2012; Ziadat and Taimeh 2013). Surface SWC is determined by a soil's physical and chemical properties as well as various terrain factors and the status of vegetation coverage (Fu et al. 2014; Wang 2007).

Ground-penetrating radar (GPR) has proven useful for monitoring surface SWC changes (Benedett 2010; Galagedara et al. 2005; Hubbard et al. 2002; Huisman et al. 2003; Ma et al. 2015). Additionally, GPR has many merits, such as a large detection area, rapid detection speed, and non-destructive detection. Compared with conventional methods, such as neutron probing and TDR, the GPR method

✉ Zhiyuan Wu
734694237@qq.com

1 Beijing Municipal Research Institute of Eco-Environmental Protection, 100037 Beijing, China

2 State Key Laboratory of Coal Resources and Safe Mining, China University of Mining and Technology, 100083 Beijing, China

3 Key Lab of Karst Environment and Geohazard, Ministry of Land and Resources, Guizhou University, 550025 Guiyang, China

avoids the labour-intensive and time-consuming point measurement methods (Anita 2006; Grote et al. 2003; Johnson et al. 2000; Ma et al. 2014). Compared with remote sensing, GPR has a high detection precision and small interference from vegetation Lunt et al. 2005; Qin et al. 2013; Wijewardana et al. 2010). Roth (2004) used 100 MHz and 250 MHz GPR to detect soil hierarchy and groundwater levels in agricultural soils and found that the GPR results in a soil profile at a depth of 1.2 m were consistent with those in an excavation profile. Ji (2011) used 100 MHz GPR to detect the water content of sandy loam at depths of 1 and 1.5 m, and found that the 100 MHz GPR could clearly decode the radar wave signal in the sandy soil; the absolute error of the 100 MHz GPR was within 0.5% compared with TDR results of 6.3 and 19.7%. Cui (2015 and 2018) used 200 MHz GPR to detect the water content of the sand layer in coal mining areas in western China, and found that GPR accurately detected the average volumetric water content of sandy soil at depths up to 10 m. Qiao (2019) used the 250 MHz GPR average envelope amplitude (AEA) method to detect the soil water content of reclaimed soil in coal mine subsidence areas, and found that the amplitude signal attribute of the GPR is significantly related to the soil water content, such that the GPR was about as accurate as actual measurements of soil water content. The lower the frequency of GPR antenna, the deeper the detection depth, the smaller the resolution of GPR information acquisition, and the lower the detection accuracy (Ji et al. 2011). Most of the previous studies are based on low-frequency GPR, which has the advantage of deep detection but inevitably affects the degree of detection. It is still unclear whether high-frequency GPR can detect soil surface water content with high accuracy and what special technical requirements it has.

Bian (2009) used remote sensing technology to analyse the factors influencing soil water content in desertified mining areas and showed that elevation is the key factor affecting the distribution of soil moisture content. Surface cracks caused by mining increase the evaporation of surface soil moisture, and the stretching and deformation of the surface easily breaks the roots of plants, which in turn affects plant growth. Yuan (2016) showed that compared to unmined areas, the soil bulk density and water content of subsided areas are significantly lower, and its porosity is significantly higher. Xu (2010) studied the distribution of SWC in a coal mining subsidence area in the plain and showed that the SWC in the unsaturated zone below 30 cm first decreases and then increases as coal mining proceeds. The cracks increase in vertically and the soil water holding rate decreases. However, the physical and chemical properties of surface soils in different subsidence areas are different Chen et al. 2014; Huang et al. 2014; Shi et al. 2017; Zhang et al. 2010;), and research regarding the combination of different coal mining subsidence and soil properties is scarce and sporadic. To determine the main factors controlling SWC changes and distribution before and after mining in different subsidence areas, we used classical statistical methods to analyse the relationships between the surface SWC and the major soil physical properties and terrain factors in different subsidence areas: total soil porosity (TSP), soil organic matter (SOM), soil clay content (SCC), (slope gradient (SG), slope aspect (SA), and vegetation density (VD). Our objectives were to research how the surface SWC changes in different subsidence areas after mining and to determine

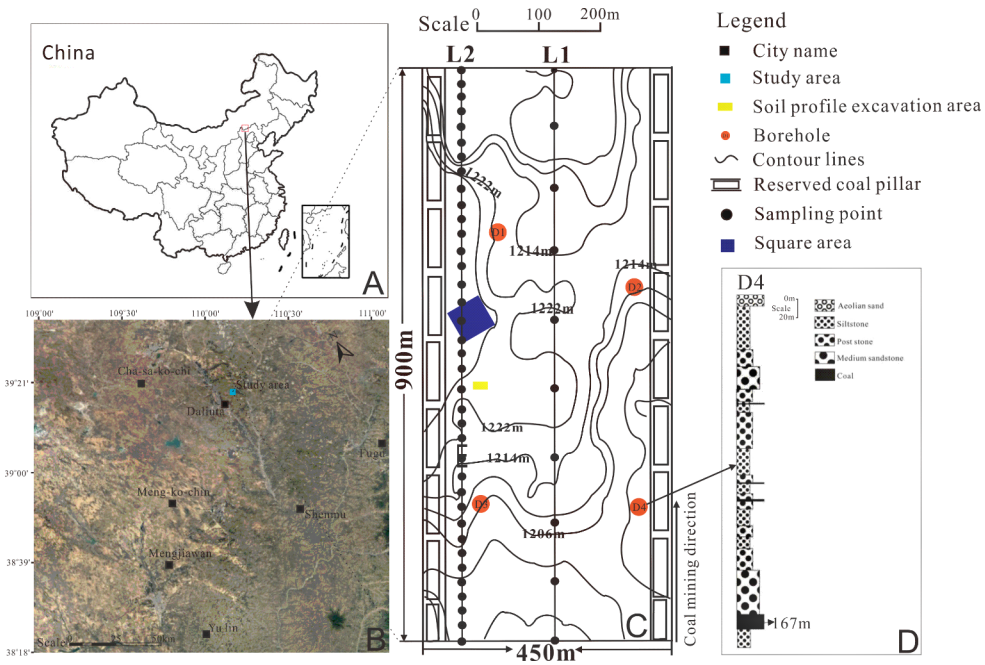

Fig. 1 A and B Study site in the Daliuta mining area; C The sampling point locations and GPR survey lines in the study area; D Lithologic column diagram of borehole D4

the main factors that control the redistribution of the surface SWC in different subsidence areas after mining.

Materials and methods

Overview of the Research Area

The selected research area was located in the Daliutang mining area of the Shendong coal mine, which is at the junction of northern Yulin, Shaanxi Province, and the southeastern Inner Mongolia Autonomous region. The geographical coordinates are longitude 110°14'05.96" and latitude 39°16'26.69" (Fig. 1). The mining area has a typical temperate semiarid continental climate, with a short (an average of 179 days) frost-free period, long freeze-up periods, and hot summers with little rain. The average annual temperature is 6.2 ~ 8.5 °C, with annual extreme temperatures in the range of 28.1 ~ 38.9 °C. Nearly 30 years of statistics show that the annual rainfall is 400 mm, and the annual evaporation is 2000 mm, so evaporation far exceeds rainfall (Nie et al. 1998; Wang et al. 2013; Zhang et al. 2010). Due to the area's dry climate, the depth of the water table is generally < 30 m. The soil types in the study area are fine sand, clay, and clay-bearing sands in the shallow strata (< 10 m), while the surface mainly consists of sand accumulation landforms, with the upper portion covered by sand bodies with depths of 0–20 m. The vegetation mainly consists of *Salix mongolica*. Due to greening efforts by the coal mine company, a small number of poplar trees are distributed throughout the research area.

The coal mining in the study area occurred from Jan. 2016 to April 2016; the working face length was 900 m. The depth of the coal seam in the study area is ≈ 200 m, and the coal seam is nearly horizontal. The lithologies of the strata above the coal seam are mainly medium sandstone, fine-grained sandstone, siltstone, and aeolian sand. The GPR detection surveys were conducted in in early winter in Nov. 2015 and 2017 to eliminate the effect of rainfall on surface SWC.

Instrument and Detection Methods

A GR-400 MHz high frequency GPR system, independently developed by China University of Mining & Technology (Beijing), was used in the field experiments. The GR system is mainly composed of one host and two antenna boxes. One of the two antenna boxes holds the transmitting antenna while the other holds the receiving antenna. The host is connected to the two antenna boxes through the antennas (Fig. 2). There were 2048 sampling points in the GPR's detection field, and the spatial resolution was 0.2 m. With a time window of 20 ns, the integrated radar wave velocity in the shallow strata was 0.125 m/ns, and the maximum penetration depth was 1.25 m.

GPR detection and sampling were mainly conducted in two areas. The first area had two 900 m long survey lines, which were named lines L1 and L2, respectively (Fig. 1 C). The measurement lines had a 30° included angle in the north direction, and the direction of the radar detection was the same as the coal mining. The second was a 40 m × 40 m square (the 1,600 m^2 purple square in Fig. 1 C) at the edge of the mining area.

First, in Nov. 2015, the GPR was conducted along the two 900 strips. The L1 line, located within the centre of the mining area and the L2 line, at the edge of the mining area, were sampled. The sampling points in the two lines included a shady slope, the adret of the dune, and a flatter region. The sampling tool was a ring sampler with a height of 10 cm and volume of 100 cm^3. Oven baking was performed indoors to test the SWC to calibrate the validity and analyse the accuracy of the SWC radar detection. Sampling was conducted at 25 m intervals with a total of 37 sampling points and 10 sampling analysis points in line L1 (Fig. 1 C). Then, the relatively flat 1,600 m^2 section was selected at the edge of the mining area to conduct radar detection and sampling. The square area GPR survey was conducted using a rectangular coordinate system with a survey line every 4 m in the X and Y directions. The positions of the survey lines were occasionally slightly changed due to the influence of vegetation, such as *Salix mongolica*. The drill hole sampling was conducted only in L1, L2, and the square area in both the 2015 and 2017 surveys. To observe the settlement of the mined area, this study set up a settlement observation line L3 in the direction of the vertical mining face and set a settlement observation point every 50 m. There were ten settlement observation points in the L3 line. The GPR survey was conducted shortly before sampling to ensure the accuracy of the SWC detected.

GPR Data Processing Method

In this study, GR radar signal processing software was used to process the GPR data. One-dimensional filtering, wavelet transform, wavelet coherence enhancement, and AGC gain processing methods were used to process the radar signal

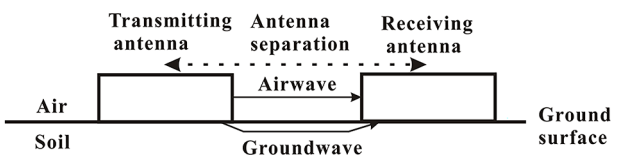

Fig. 2 Schematic diagram showing the GPR working principle with the ground wave method

to improve the longitudinal resolution of the radar signal. Mean background denoising, horizontal prediction filtering, horizontal coherence enhancement, and two-dimensional spectral inverse transformation were used to process the radar signal to improve the lateral resolution of the radar signal (Fig. 3).

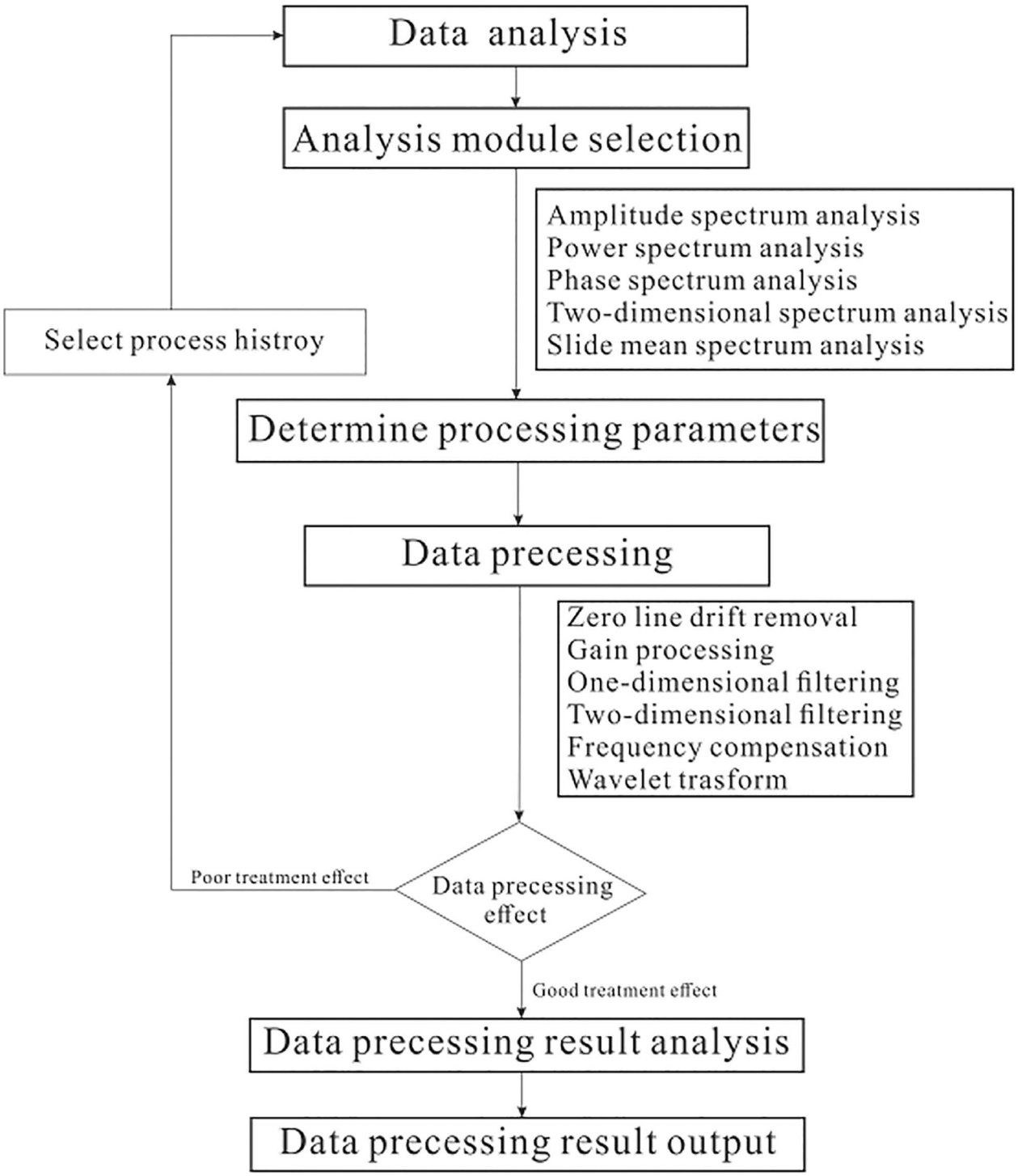

Fig. 3 GPR data processing flow chart

Soil Sample Processing and Statistical Analysis

Soil samples were collected using the ring-knife method and the soil was stored using self-sealing bags. The soil samples were sent to the laboratory on the same day. The samples were placed in the oven (the model is KLM29-CW-01) in the laboratory and baked at 105 °C for 24–48 h. After baking, the soil samples were removed and the dry weights of the soil samples were calculated; then, the SWCs were determined. The ring sampling law was adopted for the calculation of the soil bulk densities. The Pyknometer method was then used for to calculate the soil specific gravities using the results of the soil bulk density and the specific gravities were used to calculate the soil porosities. The sieving method combined with the hydrometer method was used to calculate the soil clay particle contents (Li et al. 2018). At the same time, RTK, GPS, tape measures, etc. were used to measure the elevation.

SPSS 21.0 software was used to analyse the mean and standard deviation of the measured data. Variance analysis was used to analyse the differences in average surface soil parameters under different mining conditions. All interpolated maps were produced by ArcGIS 10.5.

Results

Soil Water Changes in the Subsidence Centre

The L1 survey line runs transversely across nine sand dunes (located at 25, 142, 250, 300, 400, 450, 525, 650, 775, and 875 m), as shown in Fig. 1. The maximum elevation difference within the survey lines was 19.9 m. Based on the principle that the interference for radar wave signals within the antenna separation distance is the least when the wavelets are the clearest, two optimal antenna separation distances were determined from the effects of multiple ground-penetrating radar detection events with different antenna distances in 2015 and 2017, which were determined to be 102 and 114 cm, respectively.

The measured SWC of the ten soil samples of L1 in 2015 were compared with the SWC extracted from the corresponding radar detection (Table 1). The results showed that the SWC obtained by GPR was essentially the same as the measured SWC, with an average error of 0.008 cm^3/cm^3 and a correlation coefficient of 0.95 (Fig. 4), indicating that the 400 MHz GPR could obtain SWC values similar to the actual measurements. The GPR-detected SWC (0.082 cm^3/cm^3) was slightly larger than the measured SWC (0.074 cm^3/cm^3). This might be due to the frequent changes in the surface relief of the L1 line, which meant that the radar could not stay flush to the ground when going downhill, and because the sampling scale of the two methods was different.

The rough distribution chart of the SWC of the sand bodies above 30 cm for line L1 measured by GPR in 2015 and 2017 is shown in Fig. 5. The surface SWC changes were closely related to the sand dune distributions. The SWCs detected by GPR on the dune ridges were rather low (0.05–0.07 cm^3/cm^3), among which the peak SWCs were the smallest; the SWCs detected by GPR on the dune troughs were larger (0.07–0.12 cm^3/cm^3); the SWCs on the upwind slopes of dunes (average 0.084 cm^3/cm^3) were slightly larger than those on the leeward slopes of the dunes (average 0.081 cm^3/cm^3), and this was the same as the results of previous studies (Bian et al. 2009; Qin et al. 2013). At the lower elevation locations at the northwesternmost end of the measure line, the SWCs were slightly higher than those in the other areas. Across the two GPR detection surveys, the SWCs were basically the same; they were slightly higher in 2015 (0.084 cm^3/cm^3) than in 2017 (0.079 cm^3/cm^3), and the correlation coefficient of the SWC between the two GPR detection surveys was 0.74, as shown in Fig. 6, indicating that between the two detection events, the surface SWC in the centre area changed little. The surface subsidence values

Table 1 Comparison of SWC by GPR detection and measurement

Sampling name	2015 SWC (cm^3/cm^3)		SWC Difference(cm^3/cm^3)	Location
	GPR	Measured		
S1	0.064	0.051	0.013	Top of the slope
S2	0.075	0.054	0.021	Top of the slope
S3	0.095	0.089	0.006	Bottom of the slope
S4	0.096	0.093	0.003	Bottom of the slope
S5	0.061	0.051	0.010	Top of the slope
S6	0.107	0.099	0.008	Bottom of the slope
S7	0.085	0.080	0.006	Shady slope
S8	0.079	0.074	0.005	Shady slope
S9	0.074	0.069	0.005	Sunny slope
S10	0.080	0.077	0.004	Sunny slope
Average	0.082	0.074	0.008	-

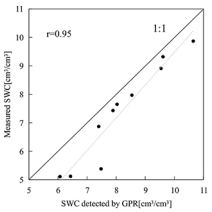

Fig. 4 Comparison of SWC detected by GPR and measured

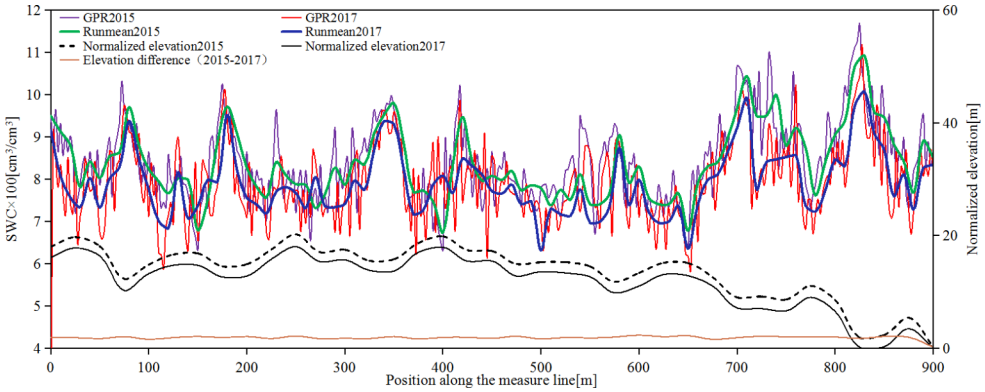

Fig. 5 Comparison of GPR-derived SWC in L1 of 2015 and 2017. The relative heights of the dunes along the GPR transect are indicated on the right axis. The green and blue lines denote a 10 m moving average of the 2015 and 2017 GPR water content data, respectively

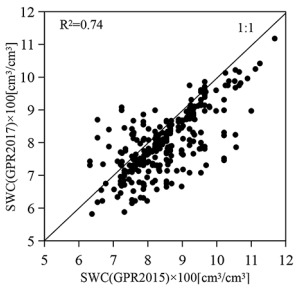

Fig. 6 Comparison of SWC by GPR in 2015 and 2017 of the L1 measure line

after mining were between 0.224 and 2.342 m, with an average reduction of 1.882 m.

Soil Water Changes in the Subsidence Boundary

SWC of L2 in 2015 and 2017

The subsidence boundary was the most drastically collapsed area. The L2 survey line was located in this area and traversed four dunes (400, 550, 700, and 875 m), which were mainly located at the northwesternmost end of the measure line; the maximum elevation difference within the line was 22 m. Figure 7 shows the rough distribution chart of the sand bodies SWCs along line L2; the surface subsidence values after mining were between 0.093 and 1.421 m, with an average reduction of 0.421 m.

The GPR-detected SWC in 2017 (average 0.083 cm^3/cm^3) was significantly less than that detected in 2015 (average 0.099 cm^3/cm^3), and the relationship between SWC and topography ceased in 2017. For example, at 400 and 550 m, the SWCs at the peaks of the dunes were 0.087 and 0.080 cm^3/cm^3, respectively, in 2017 and 0.0724 and 0.075 cm^3/cm^3, respectively, in 2015. The SWC on the dune peak increased after mining. However, the surface SWC at the trough of the dunes decreased after mining. For example, at 475 and 625 m, the SWCs at the dune trough were 0.067 and 0.094 cm^3/cm^3, respectively, in 2017, and 0.11 and 0.126 cm^3/cm^3, respectively, in 2015. This indicates that mining completely redistributed the SWC characteristics at the subsidence area boundary.

SWC in the square area in 2015 and 2017

The distribution of soil water was influenced by different factors at different scales. At a large scale, the soil water content in desert mines is mainly influenced by topography (Bian et al. 2009). At a small scale, soil physical and chemical properties, vegetation, etc., affect the SWC in the surface soil (Zou et al. 2014; Wu et al. 2019). The 1,600 m^2 square area was used to study the small-scale SWC changes in a

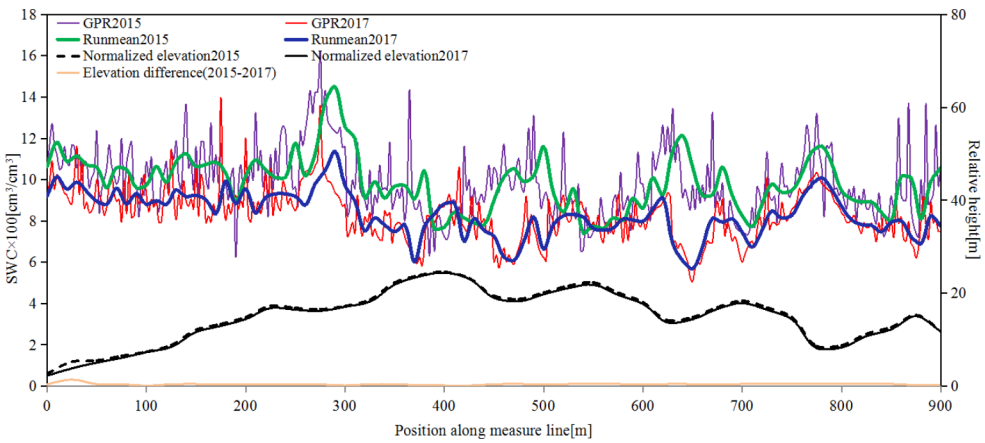

Fig. 7 Comparison of GPR and sampling-derived SWC in L2. The relative heights of the dunes along the GPR transect are indicated on the right axis. Simple data from 2015 and 2017 were measured with the surface 30 cm above the stratum. The blue line denotes a 10 m moving average of the 2017 GPR SWC data, and the green line denotes a 10 m moving average of the 2015 GPR SWC data

relatively flat area near L2. These SWCs were derived from the geostatistical software (GS+) by means of the kriging interpolation method, among which the best fitting SWC model of the half variance function was the index model in 2015 and 2017, and the R^2 values were 0.877 and 0.303, respectively, as shown in Fig. 8a and b.

The distribution of the SWC of the shallow sand bodies in the square area under the conditions of the various environmental factors is shown in Fig. 9a and b. The vegetation within the square area consists of *S. mongolica* and poplar trees. The red points are the stem positions of the poplar trees, the green points are the stem positions of the *S. mongolica*, and the black circles are the diameters of the crown coverage with the rest of the area being bare sandy soil. The SWC obtained by GPR in 2017 (the SWC was distributed between 0.056 and 0.116 cm^3/cm^3, averaging 0.082 cm^3/cm^3) was markedly less than the SWC in 2015 (when the SWC was distributed between 0.06 and 0.13 cm^3/cm^3, and averaging 0.096 cm^3/cm^3), the same as for line L2. However, the spatial distributions of the SWC in the square area in the two detection events were extremely similar, which differs from the results of line L2. The vegetation was distributed within the areas demarked by black solid lines), among which the areas with the highest SWC were located in the *S mongolica* coverage areas, e.g. at 24 (X axis)/25 (Y axis) m and 33/36 m. The areas with the least SWCs were generally bare sandy soil (within the range of the black dotted lines), at locations such as 0/4 m, 16/0 m, and 8/12 m. In addition, the surface subsidence of the square area between the two detection events averaged 0.38 m, with the subsidence being rather evenly dispersed.

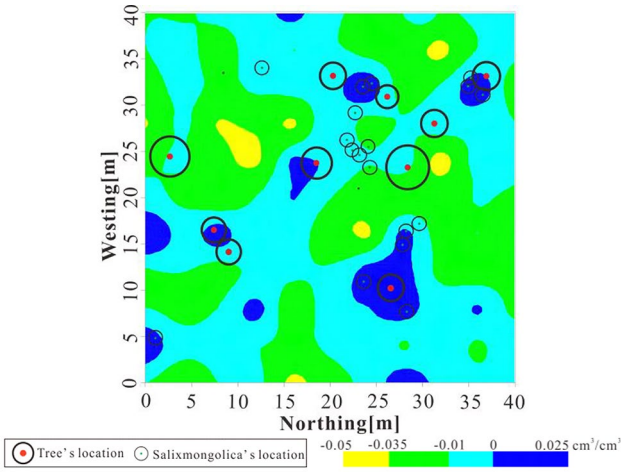

Fig. 10 Plane distribution map of SWC difference (2017 − 2015) in square area

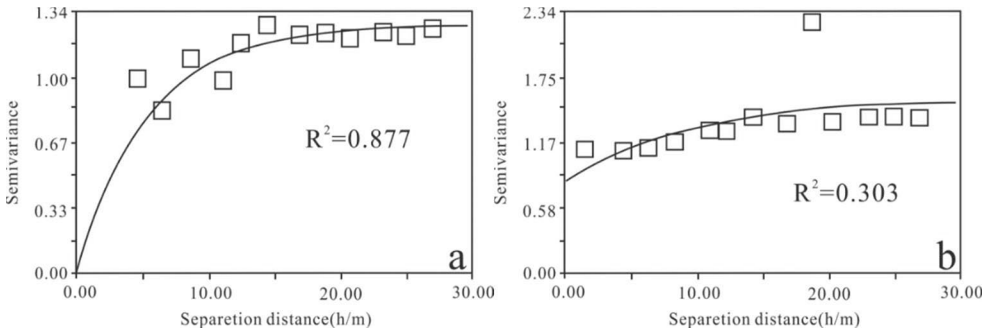

Fig. 8 SWC semi variogram in square area a 2015, b 2017

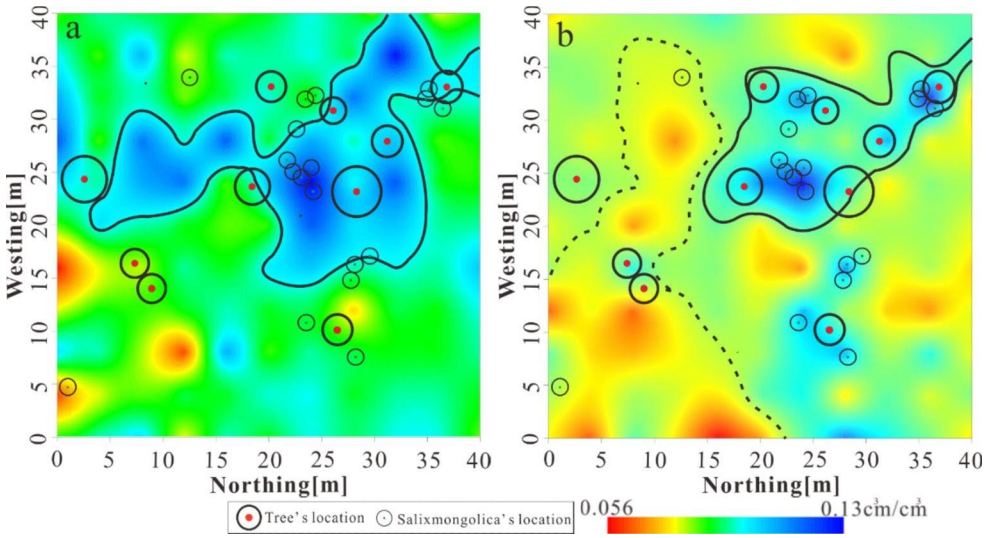

Fig. 9 Ordinary kriging interpolation of the GPR-derived soil water content: a 2015; b 2017. Note: The solid line is the SWC isoline of 0.1 cm^3/cm^3, and the dashed line is the SWC isoline of 0.08 cm^3/cm^3

The SWC difference between 2015 and 2017 in the square area is shown in Fig. 10. The SWC in the vegetated area after mining did not significantly change compared to that before mining (< 0.01 cm^3/cm^3). The SWC increased after mining in densely vegetated areas (28/12 m, 24/12 m, and 36/32 m), and the maximum increase in SWC was 0.022 cm^3/cm^3 (0 m/16 m). The vegetation coverage sufficiently maintained the surface SWC. In bare sand, except for individual areas (12/8 m, 16/40 m, and 28/0 m), the SWC on the surface after mining was generally reduced, and the SWC was reduced by up to 0.047 cm^3/cm^3 (32/24 m).

Dominant Factors Affecting Surface SWC at the Subsidence Boundary

Dominant factor of SWC distribution within L2 (900 m)

The L2 measure lines were divided into adret, shady slope, slope crest, and base, as shown in supplemental Table S1. In 2015, the correlation of the SWC and TSP in the adret was 0.445, which was significant ($p < 0.05$). The correlation of the SWC and the SCC in the shady parts was 0.799 and also significant ($p < 0.05$). However, at the top and bottom of the dunes, the SOM was the main factor influencing the SWC, with correlation coefficients of 0.690 and 0.824, respectively. In 2017, the correlation of SWC and TSP in L2 increased along the entire line. In the adret, the correlation of SWC and TSP was extremely significant ($p < 0.01$), with a correlation coefficient of 0.759. The SOM and SCC significantly influenced the SWC at the base of the dune. Therefore, it was inferred that within the *subsidence boundary*, the SWC and its distribution after mining was affected by many of the soil's physical and chemical properties. Compared with 2015, the correlation of the total soil porosity markedly increased in 2017.

Dominant factors of SWC distribution in the 1600 m^2 area

Table 2 shows the Pearson correlation analysis of the various STPs, VDs, and SWCs within the square area in 2015 and 2017. The VD significantly influenced the SWC ($p < 0.01$) with correlation coefficients of 0.76 (2015) and 0.70 (2017), and the correlation coefficients between TSP and SWC were 0.383 (2015) and 0.614 (2017), respectively. The significance level of the impact of VD on the SWC was greater than that of the STP. Bian (2009) showed that the surface SWC and the vegetation index in the Daliuta coal mining area were significantly correlated, which was what we found also. The SOM and the SCC had no significant influence on the SWC; this was different from the results of line L2, which was likely related to the scarce amount of SOM and SCC in the sandy soil. Therefore, after mining, the surface SWC within the square area was mainly influenced by the degree of VD and STP, in which VD had the greatest impact on the surface SWC. In addition, compared with 2015 and 2017, the significance of STP on the SWCs increased in 2017, and the significance of the impact of VD on the SWCs somewhat weakened in 2017.

Discussion

Different SWC change patterns were found in areas with differing subsidence. Within the 900 m L1 survey line (the subsidence centre), the SWC and its distribution before and after mining showed little change and the changes in the SWC distribution in the mined area were mainly controlled by the sand dunes (Fu and Zhao 2011). This was mainly due to the uniform settlement of the centre of the mining area; fewer cracks and faster crack closure reduced the effects of evaporation on the surface SWC (Wang 2007). Thus, the subsidence centre was determined to be the most advantageous reclamation area in the studied subsidence area. Meanwhile, the SWC at the subsidence boundary dropped drastically and the SWC distribution was disturbed. The variation coefficients of SWC increased significantly (the coefficients of variation before and after mining were 0.08 and 0.25, respectively) in the L2 survey line, and the range (A) after mining was 28.4 m, significantly more than before mining (8.21 m) in the square area. A field survey revealed that there were a large number of ladder-type cracks that could not be permanently closed on the side of the mining area; these cracks caused the surface SWC of this portion to be subject to more evaporation and infiltration, thus leading to a more drastic drop in SWC (Guo et al. 2019; Tai et al. 2016; Wu et al. 2019). Although the ladder-type cracks

Table 2 Pearson correlation analysis of soil water content with TSP, SCC, SOM, and VD

Year	2015				2017			
Soil properties and vegetation conditions	TSP	SCC	SOM	VD	TSP	SCC	SOM	VD
r	0.383**	0.119	0.113	0.76**	0.614**	-0.056	0.093	0.70**
Sig	< 0.01	0.195	0.218	< 0.01	< 0.01	0.54	0.309	< 0.01
N	121	120	121	--	121	121	121	--

Note: ** means correlation is significant at a level of 0.01, and * means correlation is significant at a level of 0.05. r is the partial correlation coefficient, and N is the number of the sampling points after deleting outliers (the sampling points in the depression and crest were deleted in the data of slope gradient and slope aspect), sig is the significant

along the boundary of the mining subsidence area were artificially filled in this study, it was still difficult for the surface SWC to recover to the original state in a short time period.

At the subsidence boundary, SCC, STP, and SOM all had affected the SWC in different areas of the dunes along the L2 survey line before mining (Han et al. 2016). However, after mining, the influence of STP on SWC in different dune areas increased, while the influence of SOM and SCC on SWC decreased. Yao et al. (2012) showed that the surface SWC in bare sand was closely related to key climatological elements but that the SWC of non-bare sand was mainly restrained by two factors: key climatological elements and vegetation density. The correlation between surface SWC and STP increased significantly in the square area after mining and decreased relative to vegetation density (but vegetation distribution still played a decisive role in SWC). This suggests that in the small area of the mining subsidence area boundary, the surface SWC after mining was affected by both the STP and vegetation density. In addition, the *S. mongolica* dominated area's SWC was greater than the poplar tree area's SWC, which indicated that larger vegetation densities are associated with higher SWC.

Soil excavation profile in the study area showed that plant roots (diameter range 0.2-3 cm) were more developed in the 0.2–0.6 m stratum (Fig. 11). Plant roots have a certain degree of water retention (Sang et al. 2020; Zeng et al. 2020). The average SWC was 0.087, 0.089, and 0.079 cm^3/cm^3 in the 0.2, 0.4, and 0.6 m strata and decreased sharply in the 0.8 and 1.0 m strata to 0.068 and 0.053 cm^3/cm^3, respectively, as shown in Fig. 12. Thus, vegetation was a key factor in controlling the SWC in the shallow sand layer of the study area.

Conclusions

The distribution of surface SWC were heavily affected by coal mining. Surface SWC detected by GPR was just as accurate as physical sampling methods. The SWC distributions were mainly controlled by the dune terrain in the

Fig. 11 Soil excavation profile in the study area

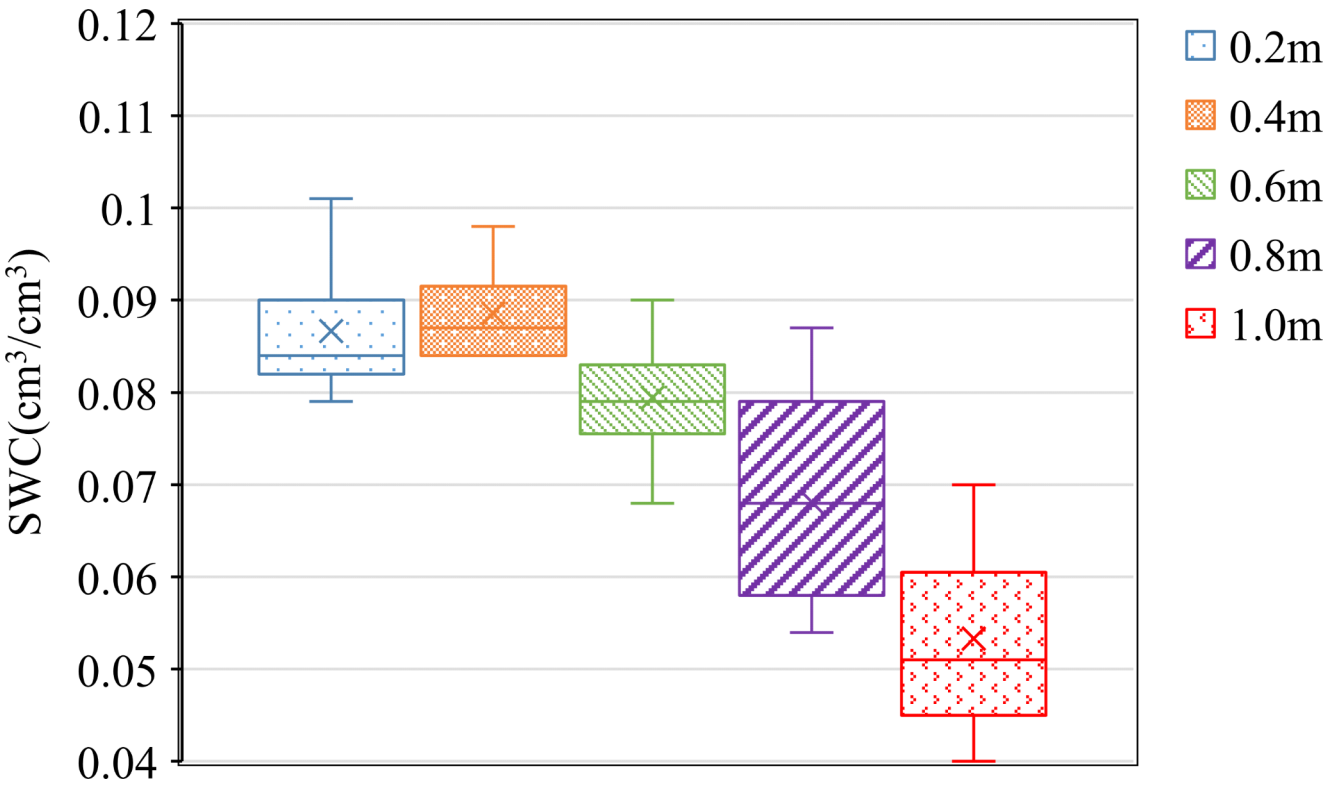

Fig. 12 Box diagram of SWC distribution at different depths of soil excavation section

subsidence centre. The SWC in the subsidence boundary area significantly decreased after mining and the correlation between the SWC and dune terrain morphology was lost. Analysis showed that the SWC was mainly influenced by changes in the TSP after mining along line L2. Within the square area, the detected SWC in 2017 (0.082 cm^3/cm^3) was obviously less than that in 2015 (0.096 cm^3/cm^3). The SWC was significantly correlated to VD and STP, and the VD had the greatest influence on the SWC.

Supplementary information The online version contains supplementary material available at https://doi.org/10.1007/s10230-022-00879-2.

Acknowledgements The authors wish to acknowledge State Key Laboratory of Coal Resources and Safe Mining, China University of Mining and Technology, Beijing for providing financial support (SKLCRSM17KFA06) and Sensors and Software Inc., for providing GPR instruments for this research.

References

Anita T (2006) Water content and porosity estimated from ground-penetrating radar and resistivity. J Appl Geophys 2(58):99–111. https://doi.org/10.1016/j.jappgeo.2005.04.004

Booth CJ (2006) Groundwater as an environmental constraint of longwall coal mining. Environ Geol 49(6):796–803. https://doi.org/10.1007/s00254-006-0173-9

Bian Z, Lei S, Chang L, Zhang R (2009) Analysis of influencing Factors of soil moisture content in Desertification mining areas based on remote sensing images. J China Coal Soc 34(4):520–525

Benedetto A (2010) Water content evaluation in unsaturated soil using GPR signal analysis in the frequency domain. J Appl Geophys 71(1):26–35. https://doi.org/10.1016/j.jappgeo.2010.03.001

Chen Z, Li Y, Deng N, Tang Z, Fan L, Wu L (2014) Effect of coal mining subsidence on soil physical properties of rice field in mountain region of southwest China. Trans CSAE 30(18):276–285

Cui F, Wu Z, Wu Y (2015) Application of GPR in the spatio-temporal variation of moisture content of sandy loam layer in western China. J China Coal Soc 40(10):2437–2444

Cui F, Chen B, Wu Z, Nie J, Geng X (2018) Soil moisture estimation based on GPR power spectrum and envelope amplitude in sandy loam. Trans CSAE 34(7):121–127

Du S (2010) The rule of the overlying strata movement and their phytoremediation technology after large-scale underground mining operation in Shengdong coal mine area. PhD Diss, China Univ of Mining and Technology (Beijing. [in Chinese]

Fu C, Zhao J (2011) Soil water distribution characteristics of different types of dune in the southeast margin of Maowusu Sandy Land. J Xi 'an U Sci Technol 28(3):377–383

Fu T, Chen H, Zhang W, Gao P, Wang K (2014) Spatial variability of soil moisture content and its influencing factors in small Karst catchment during dry period. Trans CSAE 30(14):124–131

Galagedara LW, Parkin GW, Redman JD, Bertoldi PV, Endres AL (2005) Field studies of the GPR ground wave method for estimating soil water content during irrigation and drainage. J Hydrol 301(1):182–197. https://doi.org/10.1016/j.jhydrol.2004.06.031

Grote K, Hubbard SS, Rubin Y (2003) Field-scale estimation of volumetric water content using ground-penetrating radar ground wave techniques. Water Resour Res 39(11):1–14. https://doi.org/10.1029/2003WR002045

Guo Q, Ma Z, Su N, Yang Y, Han Z (2019) Effects of cracks in coal mining subsidence area on soil moisture content in Shenfu-Dongsheng coalfield. Sci Soil Water Conserv 17(1):109–116

Huismana JA, Sperlb C, Boutena W, Verstraten JM (2001) Soil water content measurements at different scales: accuracy of time domain reflectometry and ground-penetrating radar. J Hydrol 245:48–58. https://doi.org/10.1016/S0022-1694(01)00336-5

Hubbard SS, Grote K, Rubin Y (2002) Mapping the volumetric soil water content of a California vineyard using high –frequency GPR ground wave data. Lead Edge 21(6):552–559. https://doi.org/10.1190/1.1490641

Huisman JA, Hubbard SS, Redman JD, Annan AP (2003) Measuring soil water content with ground penetrating radar: a review. Vadose Zone J 2:476–491

Huang XN, Li XJ, Liu N, Min X (2014) Characteristics of soil particles fractal dimension under different reclamation years in coal mining subsidence. J China Coal Soc 39(6):1140–1146

Han Y, Shi N, Wang Q, Quan Z (2016) Change characteristics of soil physical and chemical properties in sandstorm areas under the interference of coal mining collapse. Environ Sci Technol 11:15–19

Johnson LF, Nemani RR, Pierce LL, Bobo MR, Bosch D (2000) Toward the improved use of remote sensing and process modeling in California's premium wine industry. Proc, IEEE International Geoscience & Remote Sensing Symp, pp 363–365

Ji LQ, Zhu AN, Zhang JB, Xin XL, Li XP (2011) Determining soil water content by using low-frequency ground-penetrating radar ground wave techniques. Soils 43(1):123–129

Kratzseh IH (1986) Mining subsidence engineering. Environ Geol Water Sci 8(3):133–136

Lunt IA, Hubbard SS, Rubin Y (2005) Soil moisture content estimation using ground-penetrating radar reflection data. J Hydrol 18(307):254–269

Liu X, Bai Z, Zhou W, Cao Y, Zhang G (2017) Changes in soil properties in the soil profile after mining and reclamation in an opencast coal mine on the Loess Plateau, China. Ecol Eng 98:228–239. https://doi.org/10.1016/j.ecoleng.2016.10.078

Li B, Li L, Zhang Y, Ren Q, You H (2018) Study on the characteristics of soil texture in Shanjiankou basin. J Hebei Forestry Sci Technol 2:26–29

Ma F, Lei S, Yang S, Zhen F, Wang Y (2014) Study on the relationship between soil water content and ground penetrating radar signal attributes. Soil Sci Bull 45(4):809–815

Ma Y, Zhang Y, Zubrzycki S, Guo Y, Farhan SB (2015) Hillslope-Scale variability in seasonal frost depth and soil water content investigated by GPR on the southern margin of the sporadic permafrost zone on the Tibetan plateau. Permafr Periglac Process 26(4):321–334. https://doi.org/10.1002/ppp.1844

Nie J, Zhang G, Li J (1998) Influence of mining collapsing action on the surface ecological environment-taking Shen Mu Daliuta mine area as the study area. Site Invest Sci Technol 4:15–20

Qin Y, Chen X, Zhou K, Klenk P, Roth K, Sun L (2013) Ground-penetrating radar for monitoring the distribution of near-surface soil water content in the Gurbantunggut Desert. Environ Earth Sci 70(6):2883–2893. https://doi.org/10.1007/s12665-013-2528-3

Qiao X, Cao Y, BI R (2019) Characteristics of soil water content of reclamation farmland in mining area of the Loess Plateau based on AEA method. Chin J Soil Sci 50(1):63–69

Roth K, Wollschlager U, Cheng ZH, Bao Z (2004) Exploring soil layers and water tables with ground-penetrating radar. Pedosphere 14(3):273–282

Shi P, Zhang Y, Hu Z, Ma K, Yu B (2017) Influence mechanism of coal mining subsidence on soil quality and restoration measures in west China aeolian sand area. J U Chin Acad Sci 3:49–59

Song Y (2007) Soil water migration and environment effect in Shenfu-Dongsheng subsidence area. PhD Diss, Chinese Academy of Geological Sciences [in Chinese]

Sang K, Hu G, Huang C, Yang X, Guo E (2020) Effects of root structure characteristics of 5 plant types on soil

infiltration in the Yellow River riparian.Science of Soil and Water Conservation18(5):1–8

Tai X, Hu Z, Chen C (2016) Effect of mining subsidence fissure on moisture of surface soil in aeolian sand area. China Coal 42(8):113–117

Wang J (2007) Influence of coal mining subsidence on physical and chemical properties of sandy soil in semi-arid area. PhD Diss, Inner Mongolia Agricultural University [in Chinese]

Weihermuller L, Huisman JA, Lambot S, Herbst M, Vereecken H (2007) Mapping the spatial variation of soil water content at the field scale with different ground penetrating radar techniques. J Hydrol 340:205–216. https://doi.org/10.1016/j.jhydrol.2007.04.013

Wang Y, Shao M, Liu Z, Warrington D (2012) Regional spatial pattern of deep soil water content and its influencing factors. Int As Scien Hydrol Bull 57(2):265–281. https://doi.org/10.1080/02626667.2011.644243

Wang Q, Quan Z, Han Y, Fu M, Ye Y (2013) Effects of mining subsidence on soil properties in windy desert area. Sci Soil Water Conserv 11(6):110–118

Wei T, Chen C, Ye S, Deng X, Xie Y, Cao Y (2015) Coal mining subsidence impact on soil physical and chemical properties in windy desert area. Adv Mater Res 1092–1093:1087–1091. https://doi.org/10.4028/www.scientific.net/AMR.1092-1093.1087

Wijewardana YGNS, Galagedara LW (2010) Estimation of spatio-temporal variability of soil water content in agricultural fields with ground penetrating radar. J Hydrol 391(1–2):24–33. https://doi.org/10.1016/j.jhydrol.2010.06.036

Wu L, Tian J, Tang Y, Zhu Z (2019) Effects of collapse-fissure on soil moisture in arid and semi-arid mining areas. South-to-North Water Transfers and Water Science & Technology 3:115–120

Xu CG, Xu G, Ma Z, Wang Q, Chen Y, Xu C, Chen Y, An S (2018) Research on moisture characteristics and influencing factors of unsaturated zone in coal mining subsidence area in plain area. Underground Water 40(3):9–11

Yao G (2012) Effect of coal mining subsidence on ecological environment and recovery technique. PhD Diss, Beijing Forestry Univ [in Chinese]

Yuan Y, Chen C, Tai X, Yang K, Zhao P (2016) The effect of coal mining at super large working face on the physical and chemical properties of surface soil in windy sand area. Inner Mongol Coal Econ 3:94–95

Zhao H (2005) Research of soil water distribution and dynamic characteristic under the coal mining condition. Master Diss, Chinese Academy of Geological Science [in Chinese]

Zhang Y (2009) Study on variability of physical and chemical properties of sandy soil after coal mining subsidence. Master Diss, Inner Mongolia Agricultural Univ

Zhang Y, Wang J, Ding G, Gao Y, Yan L, He Z, Na Q, Gong P, Ren Y (2010) Variation of physic-chemical properties of Aeolian sandy soil at coal mining subsidence and its evaluation. Acta Pedol Sin 47(2):262–269. doi:https://doi.org/10.11766/trxb200811240209

Ziadat F, Taimeh A (2013) Effect of rainfall intensity, slope, land use and antecedent soil moisture on soil erosion in an arid environment. Land Degrad Develop 24(6):582–559. https://doi.org/10.1002/ldr.2239

Zou H, Bi Y, Zhu C, Du T, Han B (2014) Influence of coal mining subsidence on sandy soil moisture distribution. J Chin U Min Technol 43(3):496–501

Zeng F, Zhang W, Liu G, Zhang D, Li X, Zhang L, Yuan L, Zhang X (2020) Stable restoration approaches and sustainable management

techniques for major dominant vegetation in typical desert areas of China. J Chin Acad Sci 35(6):63–70